Structural characterization of B-doped diamond nanoindentation tips

David J. Sprouster,[a] Simon Ruffell, Jodie E. Bradby, and James S. Williams
Department of Electronic Materials Engineering, Research School of Physics and Engineering, Australian National University, Canberra, Australian Capital Territory 0200, Australia

Mark N. Lockrey and Matthew R. Phillips
Microstructural Analysis Unit, University of Technology, Sydney, Broadway, New South Wales 2007, Australia

Ryan C. Major and Oden L. Warren
Hysitron, Inc., Minneapolis, Minnesota 55344

(Received 19 July 2011; accepted 19 October 2011)

We report on the electrical and structural properties of boron-doped diamond tips commonly used for in-situ electromechanical testing during nanoindentation. The boron dopant environment, as evidenced by cathodoluminescence (CL) microscopy, revealed significantly different boron states within each tip. Characteristic emission bands of both electrically activated and nonelectrically activated boron centers were identified in all boron-doped tips. Surface CL mapping also revealed vastly different surface properties, confirming a high amount of nonelectrically activated boron clusters at the tip surface. Raman microspectroscopy analysis showed that structural characteristics at the atomic scale for boron-doped tips also differ significantly when compared to an undoped diamond tip. Furthermore, the active boron concentration, as inferred via the Raman analysis, varied greatly from tip-to-tip. It was found that tips (or tip areas) with low overall boron concentration have a higher number of electrically inactive boron, and thus non-Ohmic contacts were made when these tips contacted metallic substrates. Conversely, tips that have higher boron concentrations and a higher number of electrically active boron centers display Ohmic-like contacts. Our results demonstrate the necessity to understand and fully characterize the boron environments, boron concentrations, and atomic structure of the tips prior to performing in situ electromechanical experiments, particularly if quantitative electrical data are required.

I. INTRODUCTION

Knowledge of the physical properties of semiconductors, particularly the electrical response to an applied mechanical stimulus, is the foundation to present-day semiconductor technology. Furthermore, successful implementation of semiconductors into electronic, mechanical, magnetic, and optical devices necessitates a thorough understanding of both the electrical and mechanical properties. Recently, significant interest has grown in in-situ characterization of the electromechanical response of various semiconductor materials that undergo structural phase transformations (crystalline–crystalline or crystalline–amorphous) under extreme conditions such as pressure and/or temperature.[1,2] Such investigations are a novel means to characterize the subtle differences in electrical conductivity, from an initial-to-final phase, and to give valuable information on the transformation pathway of such materials. Nanoindentation is one such technique that can be easily used to both quantify and link the mechanical and electrical behavior of semiconductor materials and give significant insight into the deformation processes during indentation loading and unloading.[3,4]

In situ electrical characterization during the load–unload cycle of a nanoindentation experiment is made possible through the use of a conductive tip.[5,6] Recently, conductive nanoindentation tips fabricated from B-doped diamond (BDD) have been used during in-situ electromechanical characterization.[7–9] The technique has provided some qualitative measurements that have shed light on the electrical/mechanical response of several semiconductor materials[3,10] and piezoelectric materials.[11]

The dramatically improved lateral resolution (nm) and load control of modern nanoindentation systems now facilitate correlation between the mechanical and morphological data on dimensional scales comparable to atomic force microscopy based techniques,[12] but with significantly enhanced mechanical information. Such improvements in nanoindentation instrumentation allow unique electromechanical characterization of molecular and biological systems, where the coupling between electrical and mechanical phenomena is a universal feature in virtually all biological systems. Potential bioapplications include uncovering the fundamental mechanisms of the electromechanical response of cellular membranes and electromotive proteins.[13]

[a]Address all correspondence to this author.
e-mail: djs109@physics.anu.edu.au
DOI: 10.1557/jmr.2011.377

 © Materials Research Society 2011

https://doi.org/10.1557/jmr.2011.377 Published online by Cambridge University Press

Phenomenologically, when two materials are brought into contact there is a resistance associated with the constriction of electron flow through the small area. This resistance, known as the contact (or constriction) resistance R, has been derived from the principles of Ohmic conduction and electric fields by Holm[14] as

$$R = \frac{\rho_1 + \rho_2}{4r} \quad .$$

Here, ρ_1 and ρ_2 are the resistivities of material 1 and material 2, respectively, and r is the radius of the contact. Determination of r from indentation experiments is relatively straightforward by considering the tip geometry used during nanoindentation and contact area of the tip as a function of the applied load/penetration depth. As such, the measured resistance between two materials, like that in the current nanoindentation experiments discussed below, is highly dependent on the active contact area.

The implementation of conductive diamond for device fabrication in high-power transistors, high-temperature and harsh-environment device applications has been recognized for many years.[15–18] While there has been significant progress in the growth and quality of single-crystal layers, effective incorporation of electrically active p- and n-type dopants remains a main issue.[19] This is of paramount importance in nanoindentation applications where the conductive tip probes depths of a few hundred nanometers. Thus, if the electrically active area and the contact area discussed above are different due to inconsistencies in the doping profile as electrically inactive centers, or a nonuniform doping profile, the accuracy and reproducibility of any in-situ electrical measurements is limited. Thus, understanding the electrical, structural, surface, and dopant properties of the BDD tips is crucial as the electrical response of the material studied is intrinsically linked to the quality of the tip.

In the present article, we quantify various differences in the electronic and structural properties and doping profile present for several conductive BDD nanoindentation tips. These differences are then used to discuss the electrical response of the tips used to indent gold films and glassy carbon substrates. The different atomic B environments and near-surface homogeneity of active B doping within each tip was quantified via cathodoluminescence (CL) spectroscopy and CL mapping, whereas Raman microspectroscopy was used to determine the structural characteristics on the atomic scale and to estimate the B concentration of the BDD tips.

II. EXPERIMENTAL

All indentations were performed using a Hysitron TriboIndenter (Minneapolis, MN) fitted with 11 different BDD tips for the "nanoECR" mode of operation (the conductive tips were all commercially bought from Hysitron and were boron doped to a nominal resistivity of 3.3 Ω-cm). These conductive tips allow through-tip electrical measurements whereby the current can be monitored during loading/unloading, and current–voltage (*IV*) characteristics can be determined at any point on the load/unload cycles. Two bulk electrical standards were used to investigate the different BDD tips, specifically a 1.5 μm Au film deposited on a Si substrate and a thick conductive glassy carbon (800 μm) sample. The latter standard is known to show almost purely elastic mechanical response to nanoindentation (consequently with no pile up) for Berkovich indentation at the loads up to ~10 mN used here.[20] The indentation experiments were run consecutively in each sample, with no environmental changes to limit the effects of humidity and sample contamination. The electrical resistivity of the glassy carbon standard was metallic-like ($\sim 6 \times 10^{-4}$ Ω-m) as confirmed by the four-point probe technique.

CL spectra and maps were collected using an FEI Quanta 200 scanning electron microscope (SEM) equipped with a Gatan MonoCL3 system. The CL signal was detected using either an Ocean Optics QE65000 optical charge coupled device (CCD, Renens/Lausanne, Switzerland) spectrometer or a Hamamatsu R94302 Peltier cooled photomultiplier tube (Hamamatsu Photonics, Shizuoka, Japan). The wide spectral range of the CL system used, from the ultraviolet (UV) (~200 nm) to far infrared (1000 nm), allows the characterization of the major defect structures in diamond. Spatially resolved spectral maps were generated using a Moran Scientific system (Goulburn, Australia) attached to the SEM-CL set up. CL and SEM images were recorded at liquid nitrogen temperature (LNT). All CL spectra were corrected for the detection response of the system. Acceleration voltages of 10 and 15 kV corresponding to excitation depths of ~0.5–0.8 μm in diamond were used to produce sufficient CL signal. Raman microspectroscopy measurements at room temperature were made using a Jobin-Yvon T64000 instrument (HORIBA Jobin-Yvon, Longjumeau Cedex, France) fitted with an LNT-cooled CCD detector. Spectra were acquired at a short working distance (100× objective aperture) with a HeNe laser (632.8 nm) focused to a spot of 2 μm in diameter.

III. RESULTS AND DISCUSSION

A. In situ electrical properties

Figure 1 shows the through-tip *IV* curves at various positions on the loading cycle in the Au film (a, b) and in glassy carbon substrates (c, d). The load versus penetration depth curves for each material are shown as insets. The mechanical response for both tips is comparable (slight differences in the penetration depth are due to differences in tip wear), in contrast to the electrical responses, which differ significantly. For ease of discussion, the tips that show more rectifying *IV* curves are henceforth labeled as "family S" and those that show more Ohmic-like *IV* curves (almost linear *IV* curves) are labeled as "family O." Note that the Ohmic-like *IV* curves in Figs. 1(b) and 1(d) do not

https://doi.org/10.1557/jmr.2011.377 Published online by Cambridge University Press

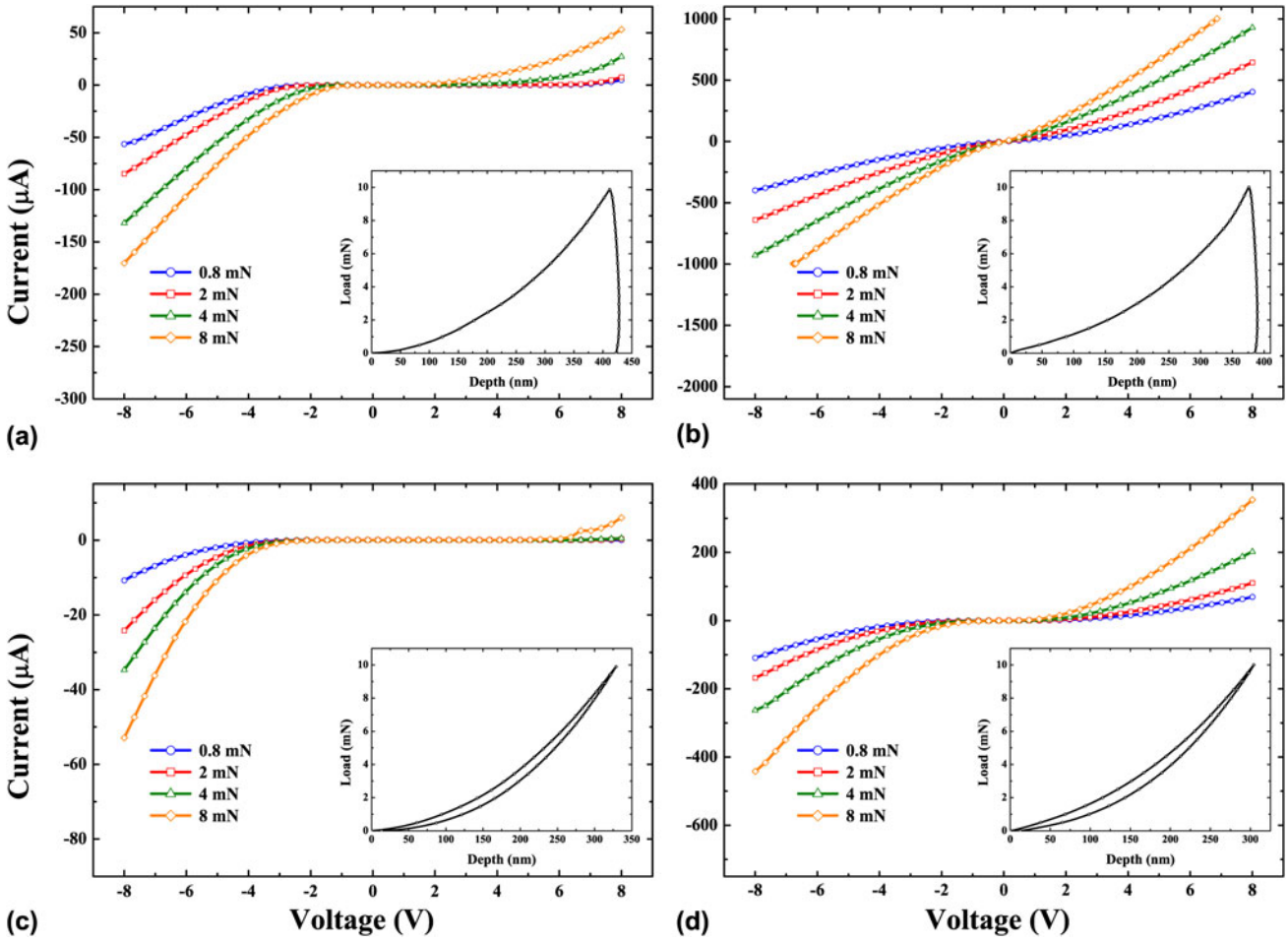


FIG. 1. Current–voltage curves extracted at loads of 0.8, 2, 4, and 8 mN for a (a, c) family S and (b, d) family O tips in (a, b) gold; and (c, d) glassy carbon standards. The insets show the load versus penetration depth curves.

exhibit the expected linear *IV* characteristics since at low loads the contact area is small resulting in the departure from pure Ohmic behavior at low voltages.[5] Fang and coworkers have also observed non-Ohmic *IV* curves while indenting bulk Cu.[8] The origins of the nonlinear electrical properties were not, however, investigated in the aforementioned study and were attributed to either surface oxidation or doping nonuniformities in the BDD tips.

The electrical properties of BDD, like other semiconductors, are principally governed by the dopant concentration.[18] For B concentrations below $\sim 10^{19}$ cm^{-3}, the high bonding energy of the B acceptors results in only a small fraction (0.2%) of ionized B donors at room temperature. Hence, in this concentration range semiconducting (i.e., Schottky) contacts dominate when the tips are brought into contact with metal-like substrates. In the intermediate doping range (10^{19}–10^{20} cm^{-3}), current conduction is dominated by nearest neighbor hopping, and for B concentrations $\sim 2 \times 10^{20}$ cm^{-3} the diamond is degenerate or metal-like. Our observation of rectifying *IV* curves of "family S" tips is similar to the electrical response commonly observed for metal–semiconductor (Schottky) diamond contacts,[21] due to a low active B concentration, typically below 10^{19} cm^{-3}. The Ohmic-like properties of family O tips are similar to our previous reports,[5] indicative of a higher active B concentration, typically above 10^{20} cm^{-3} in these tips.

B. Cathodoluminescence spectroscopy

Representative CL spectra collected over an area of 25×25 μm^2 for the different BDD and undoped diamond tips at LNT are shown in Fig. 2. Several distinct bands are visible in the undoped tip at high magnification, and these are commonly observed for various nitrogen (N)-related defects in diamond.[22–26] The absence of the free exciton bands and phonon replicas below 300 nm is attributed to N-related nonradiative recombination channels quenching their emission.[27,28] The structural integrity of the undoped diamond tip is evident, with no visible band at 430 nm indicative of dislocations/grain boundaries.[29]

The BDD tips show less fine structure in the CL signal compared to the undoped diamond tip. Vastly different

https://doi.org/10.1557/jmr.2011.377 Published online by Cambridge University Press

broad bands are visible in Fig. 2, and these clearly indicate considerably different defect states within the BDD tips. The lack of any N-related bands (compared to the undoped tip) indicates that N contamination in the BDD tips is below the detection limit of CL. The CL emission from the family S tip is lower in intensity compared to the family O tip. This difference in intensity between the two families was consistently observed for the various BDD tips, with family O tips always showing higher signals. The UV bands (at ~250 nm) shown in Fig. 2(b) are attributed to the free exciton recombination bands[27,30,31] common to diamond. The differences in the free exciton recombination band heights observable between family S and O tips are attributed to different B concentrations.[30] The relatively featureless, broad blue band centered at ~360 nm is the main band evident in the family S tips. This band has previously been observed in heavily BDD films grown by chemical vapor deposition in a very high concentration region where phase separation has been observed to occur, and also in BDD with low levels of electrically activated B.[32,33] The presence of this band indicates that there is a significant component of nonactive B[34] or B-rich clusters[35,36] in the family S tips.

The broad band at 520 nm observed in the family O tips is commonly observed for BDD films.[37] This band has been studied in detail for various natural, CVD, and high-pressure/high-temperature grown diamond samples[24,37,38] and is found to occur in regions with high active B concentration and is unaffected by the N content.[34,39] The lack of this band in the family S tips again indicates that the B present in these tips is (largely) not electrically activated. The small, broad shoulder band at 360 nm is an evidence that family O tips also contain some electrically inactive B component.

C. Cathodoluminescence mapping

The luminescence from the family O tips was further examined by performing CL mapping. Family S tips were omitted in this study due to significant charging and weak signals. Figure 3 shows an (a) SEM and (b) corresponding full spectral CL map recorded at LNT for a representative family O tip. The near-surface luminescence is clearly nonuniform with a mosaic-like texturing apparent across the whole surface. Upon close inspection, it was found that these lighter regions (not visible in the SEM image) vary

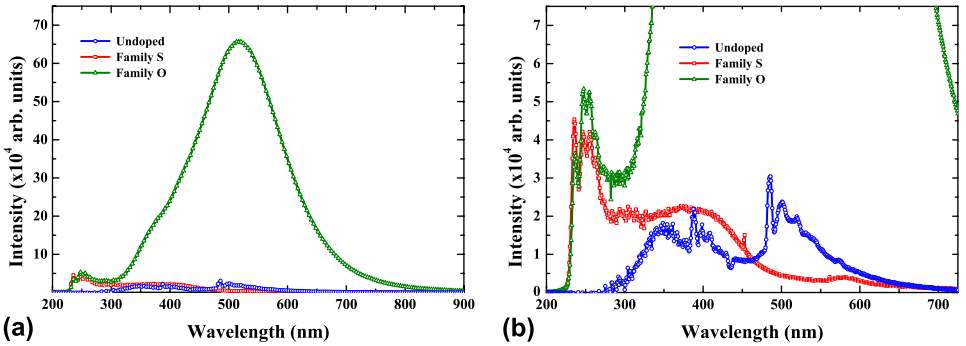


FIG. 2. (a) CL spectra recorded at liquid nitrogen temperature (LNT) for an undoped diamond tip and the BDD tips at an acceleration voltage of 15 kV and (b) the same data enlarged to highlight details of the undoped and family S tips.

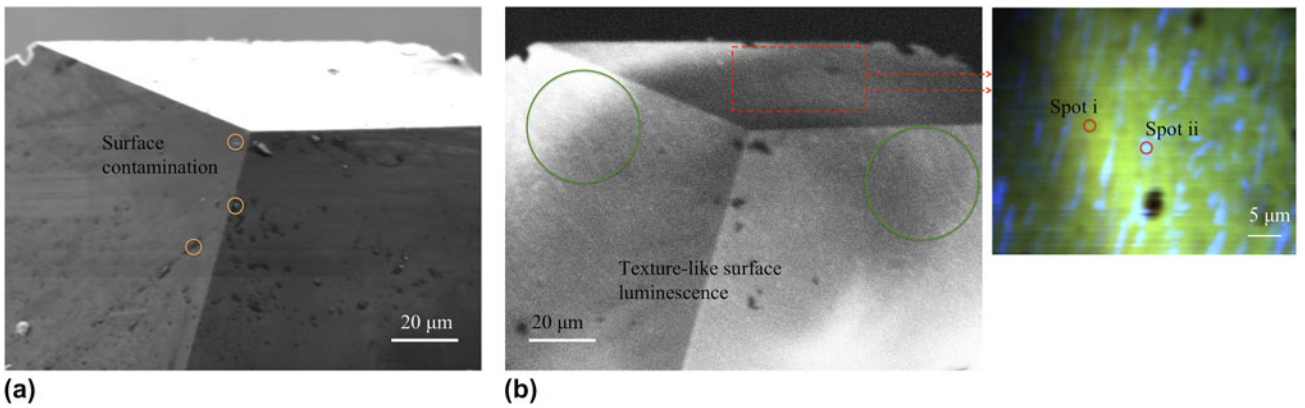


FIG. 3. (a) Scanning electron microscope and (b) spectral cathodoluminescence (CL) map recorded at LNT and with an acceleration voltage of 10 kV for a representative family O tip. The orange and green circles in (a) and (b) highlight surface contaminants and nonuniform surface luminescence, respectively. The colors in the pseudocolor map are identical to those discussed in the text. The CL spectra from the regions labeled "spot i" and "spot ii" in the inset are shown in Fig. 4.

https://doi.org/10.1557/jmr.2011.377 Published online by Cambridge University Press

greatly in size with widths ranging from 0.5 to 1.5 μm. Some of the darker regions in the CL image (many also observed in the SEM image) are attributed to surface contamination.

To investigate the origin of the nonuniform luminescent behavior, pseudocolor maps were generated over a smaller (and relatively contaminant free) region of the tip, as shown in the inset of Fig. 3. Such a technique is highly advantageous, with each individual pixel containing a single CL spectrum. As a result, more quantitative CL information can be extracted from the tip surface. The normalized CL spectra extracted from the green background (spot i), blue streak (spot ii), as indicated in the inset of Fig. 3, and the complete spectra from the full spectral image are shown in Fig. 4. The spectra from the full spectral image again show that the CL emission is dominated by the broad green band at 520 nm with the appearance of a small, but distinct blue shoulder band at 360 nm. Spectra taken from the blue streaks (spot ii) show a mixture of both green and a higher intensity 360 nm blue band compared to both spot i (which predominately contains the green band) and the background. The presence of this blue band thus indicates that the near-surface of the family O tips does contain regions high in electrically inactive centers. Furthermore, the presence of these "electrically dead" surface regions potentially hinders a quantitative analysis of through-tip electrical measurements with such tips.

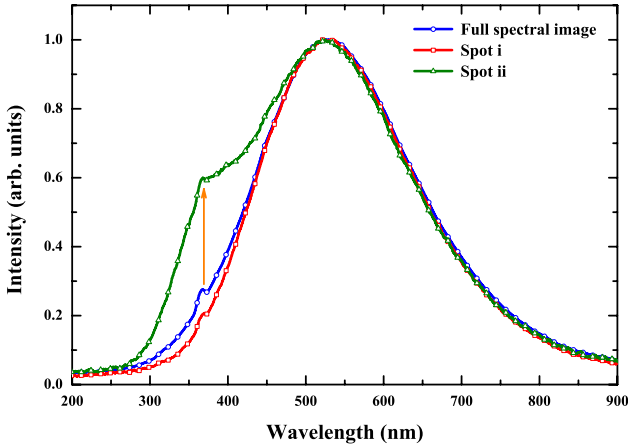


FIG. 4. CL spectra recorded at LNT from the regions shown in the inset of Fig. 3 for the family O tip.

D. Raman microspectroscopy

Figure 5 shows normalized Raman spectra collected for the undoped and representative BDD tips from families S and O. All tips show an intense zero center band (0^{Γ}) located at ~1332 cm^{-1} in agreement with previous studies.[40] Family O tips appear to have a sharper 0^{Γ} band compared to the undoped and family S tips, and this has previously been observed for polycrystalline BDD films with high B concentrations (~10^{20} cm^{-3}).[41] Another feature evident in the Raman spectra of all BDD tips are the broad, low-intensity bands centered at 592, 920, 1029, 1371, and 1475 cm^{-1}. The presence of these bands is consistent with previous Raman studies of homoepitaxial BDD layers[42] and in polycrystalline BDD films.[43,44] They occur over a wide (active) B concentration range

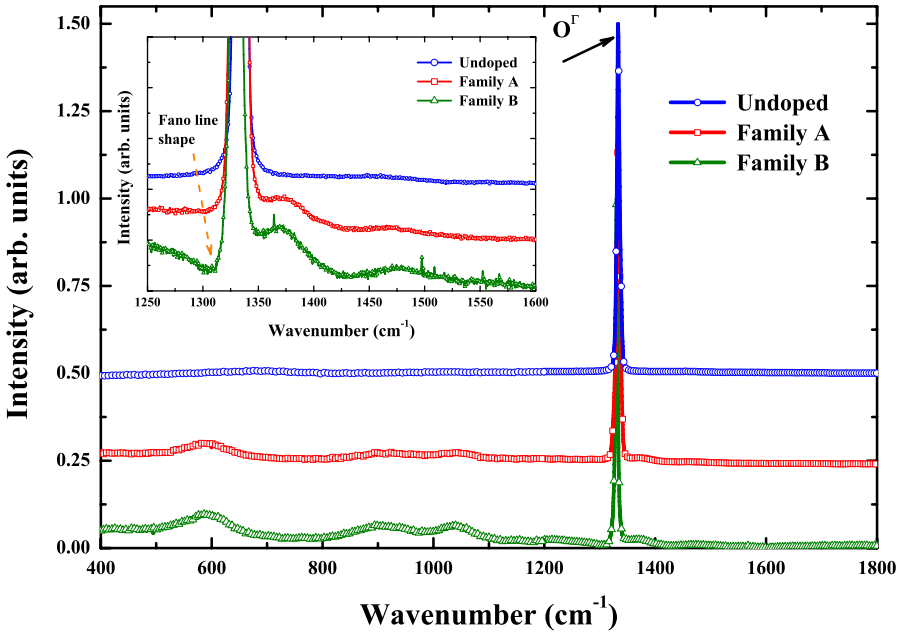


FIG. 5. Raman spectra for undoped, family S, and family O tips. All spectra have been normalized (to the 0^{Γ} band height) and offset for clarity. The inset shows the extended region from 1300 to 1600 cm^{-1}, more clearly displaying the broad bands discussed in the text.

https://doi.org/10.1557/jmr.2011.377 Published online by Cambridge University Press

TABLE I. Refined Lorentzian fitting parameters for Raman spectra shown in Fig. 5.

Sample	0^{Γ} (cm^{-1})	FWHM (cm^{-1})
Undoped	1333.2	5.7
Family S	1332.2	7.6
Family O	1330.4	4.6

FWHM, full width at half maximum.

of 10^{18}–10^{20} cm^{-3}. At still higher concentrations ($>2 \times 10^{20}$ cm^{-3}), further changes have been reported in the Raman signal and include the disappearance of the aforementioned low-intensity bands, a decrease in the intensity of the 0^{Γ} band and the emergence of new bands at 500 and 1225 cm^{-1}. The origin of the broad band at 500 cm^{-1} has recently been attributed to the formation of electrically inactive B dimers and/or large B clusters in very heavily doped diamond.[45,46]

The 0^{Γ} band of each tip shown in Fig. 5 was fitted with a Lorentzian function, and the results are given in Table I. As Table I demonstrates, relative to undoped diamond a shifting in the position of 0^{Γ} to lower wave number is observed in the family O tip. A substantial narrowing of the 0^{Γ} bandwidth is also observable in the family O tips. These are common features of all family O tips studied. The narrowing of the 0^{Γ} bandwidth is commonly observed in heavily BDD.[47,48] The 0^{Γ} band narrowing is accompanied by a small depression in intensity on the lower side of 0^{Γ}, and this change in the line shape typically occurs in heavily doped semiconductors and is referred to as the "Fano effect."[49] Furthermore, the Fano 0^{Γ} band shape begins to occur in BDD with concentrations greater than 10^{19} cm^{-3}.[47,48] It is interesting that, relative to undoped diamond, the family S 0^{Γ} band shows a much smaller shift than family O tips, but exhibits substantial peak broadening in contrast to narrowing observed for family O tips.

The analysis of the 0^{Γ} band, peak width deviations, and Fano shape obtained by Raman complement the CL data presented above, whereby the position and intensity of the bands allow us to estimate the B concentration in each tip. Family S tips, with low CL signal, broad low-intensity Raman bands and no Fano shape in the 0^{Γ} band, thus have low active B concentrations up to $\sim 10^{18}$ cm^{-3}. Family O tips, with intense CL signal and a sharper 0^{Γ} band exhibiting the Fano effect in Raman spectra, have high active B concentrations of $\sim 10^{19}$–10^{20} cm^{-3}.

IV. CONCLUSION

The B electrical activity, surface heterogeneity, local structure at the atomic level, and estimates of overall B concentrations of the different BDD tips were studied by employing a combination of characterization techniques including CL spectroscopy, CL mapping, and Raman microspectroscopy. The CL and Raman studies demonstrate that each tip family has significantly different active B concentrations. The lower CL signal, B environment, and atomic structure inferred from the Raman analysis indicate that the family S tips contain low levels of electrically active B and low overall B concentrations. Consequently, the rectifying electrical properties of indents into Au and glassy carbon can be understood in terms of low active B concentration and subsequent Schottky electrical contacts with metal-like substrates. The Ohmic-like electrical properties of the family O tips were the result of a much larger number of electrically active B and overall higher B concentrations. The high active B concentrations were identified from the intensity of the 520 nm CL band and a narrowing and shifting to lower wave numbers in the 0^{Γ} Raman band. CL mapping showed that the surface of family O tips also contained inhomogeneities in the form of regions that were low in electrically active B concentration. Our study demonstrates that a priori knowledge of the B electrical activity and atomic structure, as well as the overall B concentration, is essential prior to any in situ electromechanical testing, if quantitative electrical data is required. Alternatively, other hard tips with uniformly high conductivity could be used.

ACKNOWLEDGMENTS

This research was supported by an Australian Research Council Linkage project. JB is the recipient of an Australian Research Council QEII Fellowship.

REFERENCES

1. M.I. Eremets, V.V. Struzhkin, H-K. Mao, and R.J. Hemley: Superconductivity in boron. *Science* **293**, 272 (2001).
2. J.M. Besson, E.H. Mokhtari, J. Gonzalez, and G. Weill: Electrical properties of semimetallic silicon III and semiconductive silicon IV at ambient pressure. *Phys. Rev. Lett.* **59**, 473 (1987).
3. R. Nowak, D. Chrobak, S. Nagao, D. Vodnick, M. Berg, A. Tukiainen, and M. Pessa: An electric current spike linked to nanoscale plasticity. *Nat. Nanotechnol.* **4**, 287 (2009).
4. J.E. Bradby, J.S. Williams, and M.V. Swain: In situ electrical characterization of phase transformations in Si during indentation. *Phys. Rev. B* **67**, 085205 (2003).
5. S. Ruffell, J.E. Bradby, J.S. Williams, and O.L. Warren: An in situ electrical measurement technique via a conducting diamond tip for nanoindentation in silicon. *J. Mater. Res.* **22**, 578 (2007).
6. A.B. Mann, D. van Heerden, J.B. Pethica, and T.P. Weihs: Size-dependent phase transformations during point loading of silicon. *J. Mater. Res.* **15**, 1754 (2000).
7. S. Ruffell, K. Sears, A.P. Knights, J.E. Bradby, and J.S. Williams: Experimental evidence for semiconducting behavior of Si-XII. *Phys. Rev. B* **83**, 075316 (2011).
8. L. Fang, C.L. Muhlstein, J.G. Collins, A.L. Romasco, and L.H. Friedman: Continuous electrical in situ contact area measurement during instrumented indentation. *J. Mater. Res.* **23**, 2480 (2008).
9. N. Fujisawa, S. Ruffell, J.E. Bradby, J.S. Williams, B. Haberl, and O.L. Warren: Understanding pressure-induced phase-transformation

https://doi.org/10.1557/jmr.2011.377 Published online by Cambridge University Press

behavior in silicon through in situ electrical probing under cyclic loading conditions. *J. Appl. Phys.* **105**, 106111 (2009).
10. S. Ruffell, J.E. Bradby, N. Fujisawa, and J.S. Williams: Identification of nanoindentation-induced phase changes in silicon by in situ electrical characterization. *J. Appl. Phys.* **101**, 083531 (2007).
11. M. Bhaskaran, S. Sriram, S. Ruffell, and A. Mitchell: Nanoscale characterization of energy generation from piezoelectric thin films. *Adv. Funct. Mater.* **21**, 2251 (2011).
12. Hysitron: TI-950-TriboIndenter. http://www.hysitron.com/products/ti-series/ti-950-triboindenter.
13. S.V. Kalinin, B.J. Rodriguez, S. Jesse, E. Karapetian, B. Mirman, E.A. Eliseev, and A.N. Morozovska: Nanoscale electromechanics of ferroelectric and biological systems: A new dimension in scanning-probe microscopy. *Annu. Rev. Mater. Res.* **37**, 189 (2007).
14. R. Holm: *Electric Contacts; Theory and Applications* (Springer, New York, 2000).
15. T. Tachibana, B.E. Williams, and J.T. Glass: Correlation of the electrical properties of metal contacts on diamond films with the chemical nature of the metal-diamond interface. i. gold contacts: A non-carbide-forming metal. *Phys. Rev. B* **45**, 11968 (1992).
16. T. Tachibana, B.E. Williams, and J.T. Glass: Correlation of the electrical properties of metal contacts on diamond films with the chemical nature of the metal-diamond interface. ii. Titanium contacts: A carbide-forming metal. *Phys. Rev. B* **45**, 11975 (1992).
17. R.J. Trew, J.B. Yan, and P.M. Mock: The potential of diamond and SiC electronic devices for microwave and millimeter-wave power applications. *Proc. IEEE* **79**, 598 (1991).
18. K. Thonke: The boron acceptor in diamond. *Semicond. Sci. Technol.* **18**, S20 (2003).
19. N. Tumilty, J. Welch, R. Lang, C. Wort, R. Balmer, and R.B. Jackman: An impedance spectroscopic investigation of the electrical properties of delta-doped diamond structures. *J. Appl. Phys.* **106**, 103707 (2009).
20. N. Iwashita, M.V. Swain, J.S. Field, N. Ohta, and S. Bitoh: Elasto-plastic deformation of glass -like carbons heat-treated at different temperatures. *Carbon* **39**, 1525 (2001).
21. P.K. Baumann and R.J. Nemanich: Electron affinity and Schottky barrier height of metal–diamond (100), (111), and (110) interfaces. *J. Appl. Phys.* **83**, 2072 (1998).
22. A.T. Collins, A. Connor, C.H. Ly, A. Shareef, and P.M. Spear: High-temperature annealing of optical centers in type-i diamond. *J. Appl. Phys.* **97**, 083517 (2005).
23. A.T. Collins and G.S. Woods: Cathodoluminescence from giant platelets, and of the 2.526 eV vibronic system, in type Ia diamonds. *Philos. Mag. B* **45**, 385 (1982).
24. P.B. Klein, M.D. Crossfield, J.A. Freitas Jr., and A.T. Collins: Donor-acceptor pair recombination in synthetic type-iib semiconducting diamond. *Phys. Rev. B* **51**, 9634 (1995).
25. L.H. Robins, L.P. Cook, E.N. Farabaugh, and A. Feldman: Cathodoluminescence of defects in diamond films and particles grown by hot-filament chemical-vapor deposition. *Phys. Rev. B* **39**, 13367 (1989).
26. M. Kadri, D. Araujo, M. Wade, A. Deneuville, and E. Bustarret: Effect of oxygen on the cathodoluminescence signal from excitons, impurities and structural defects in homoepitaxial (100) diamond films. *Diamond Relat. Mater.* **14**, 566 (2005).
27. L.H. Robins, E.N. Farabaugh, and A. Feldman: Cathodoluminescence spectroscopy of free and bound excitons in chemical-vapor-deposited diamond. *Phys. Rev. B* **48**, 14167 (1993).
28. H. Sternschulte, J. Horseling, T. Albrecht, and K. Thonke: Characterization of doped and undoped CVD-diamond films by cathodoluminescence. *Diamond Relat. Mater.* **5**, 585 (1996).
29. D. Takeuchi, H. Watanabe, S. Yamanaka, H. Okushi, H. Sawada, H. Ichinose, T. Sekiguchi, and K. Kajimura: Origin of band-A emission in diamond thin films. *Phys. Rev. B* **63**, 245328 (2001).
30. H. Kawarada, H. Matsuyama, Y. Yokota, T. Sogi, A. Yamaguchi, and A. Hiraki: Excitonic recombination radiation in undoped and boron-doped chemical-vapor-deposited diamonds. *Phys. Rev. B* **47**, 3633 (1993).
31. H. Kawarada, Y. Yokota, and A. Hiraki: Intrinsic and extrinsic recombination radiation from undoped and boron-doped diamonds formed by plasma chemical vapor deposition. *Appl. Phys. Lett.* **57**, 1889 (1990).
32. R.J. Graham, T.D. Moustakas, and M.M. Disko: Cathodoluminescence imaging of defects and impurities in diamond films grown by chemical vapor deposition. *J. Appl. Phys.* **69**, 3212 (1991).
33. S. Koizumi, K. Watanabe, M. Hasegawa, and H. Kanda: Ultraviolet emission from a diamond pn junction. *Science* **292**, 1899 (2001).
34. S.C. Lawson, H. Kanda, H. Kiyota, T. Tsutsumi, and H. Kawarada: Cathodoluminescence from high-pressure synthetic and chemical-vapor-deposited diamond. *J. Appl. Phys.* **77**, 1729 (1995).
35. P. Muret and M. Wade: Acceptor compensation by dislocations related defects in boron doped homoepitaxial diamond films from cathodoluminescence and Schottky diodes current-voltage characteristics. *Phys. Status Solidi A* **203**, 3142 (2006).
36. C. Baron, A. Deneuville, M. Wade, F. Jomard, and J. Chevallier: Cathodoluminescence measurements on heavily boron doped homoepitaxial diamond films and their interfaces with their Ib substrates. *Phys. Status Solidi A* **203**, 544 (2006).
37. H. Kawarada, Y. Yokota, Y. Mori, K. Nishimura, and A. Hiraki: Cathodoluminescence and electroluminescence of undoped and boron-doped diamond formed by plasma chemical vapor deposition. *J. Appl. Phys.* **67**, 983 (1990).
38. P.J. Dean: Bound excitons and donor-acceptor pairs in natural and synthetic diamond. *Phys. Rev.* **139**, A588 (1965).
39. J. Ruan, K. Kobashi, and W.J. Choyke: On the "band-A" emission and boron related luminescence in diamond. *Appl. Phys. Lett.* **60**, 3138 (1992).
40. D.S. Knight and W.B. White: Characterization of diamond films by Raman spectroscopy. *J. Mater. Res.* **4**, 385 (1989).
41. K. Nishimura, K. Das, and J.T. Glass: Material and electrical characterization of polycrystalline boron-doped diamond films grown by microwave plasma chemical vapor deposition. *J. Appl. Phys.* **69**, 3142 (1991).
42. M. Mermoux, F. Jomard, C. Tavars, F. Omns, and E. Bustarret: Raman characterization of boron-doped 111 homoepitaxial diamond layers. *Diamond Relat. Mater.* **15**, 572 (2006).
43. M. Mermoux, B. Marcus, G.M. Swain, and J.E. Butler: A confocal Raman imaging study of an optically transparent boron-doped diamond electrode. *J. Phys. Chem. B* **106**, 10816 (2002).
44. S. Szunerits, M. Mermoux, A. Crisci, B. Marcus, P. Bouvier, D. Delabouglise, J.P. Petit, S. Janel, R. Boukherroub, and L. Tay: Raman imaging and Kelvin probe microscopy for the examination of the heterogeneity of doping in polycrystalline boron-doped diamond electrodes. *J. Phys. Chem. B* **110**, 23888 (2006).
45. E. Bourgeois, E. Bustarret, P. Achatz, F. Omnes, and X. Blase: Impurity dimers in superconducting B-doped diamond: Experiment and first-principles calculations. *Phys. Rev. B* **74**, 094509 (2006).
46. J.P. Goss and P.R. Briddon: Theory of boron aggregates in diamond: First-principles calculations. *Phys. Rev. B* **73**, 085204 (2006).
47. J.W. Ager III, W. Walukiewicz, M. Mc Cluskey, M.A. Plano, and M.I. Landstrass: Fano interference of the Raman phonon in heavily boron-doped diamond films grown by chemical vapor deposition. *Appl. Phys. Lett.* **66**, 616 (1995).
48. P. Gonon, E. Gheeraert, A. Deneuville, F. Fontaine, L. Abello, and G. Lucazeau: Characterization of heavily B-doped polycrystalline diamond films using Raman spectroscopy and electron spin resonance. *J. Appl. Phys.* **78**, 7059 (1995).
49. F. Pruvost and A. Deneuville: Analysis of the Fano in diamond. *Diamond Relat. Mater.* **10**, 531 (2001).

https://doi.org/10.1557/jmr.2011.377 Published online by Cambridge University Press